Slicing the Shadowing Uncertainty: A Measurement-Based Critical Study of Spatially Correlated Gaussian Models of Shadow Fading

Nikos Perpinias, Alexandros Palaios, Janne Riihijärvi, Petri Mähönen
Institute for Networked Systems, RWTH Aachen University, Aachen, Germany
email: {npe, apa, jar, pma}@inets.rwth-aachen.de

***Abstract*—We report results from extensive measurements based study to understand the shadow fading correlations. We have particularly studied and analyzed common assumptions done in literature for shadow fading, which is typically modeled as a spatially correlated Gaussian random process in the logarithmic scale. We show that these assumptions, starting from the Gaussianity of the radio propagation environment, do not always hold. We then discuss the assumptions regarding spatial correlations, usually taken to depend only on the distance between the points and assuming that these correlations remain the same throughout the area under consideration. This is done by comparing received power measurements for two different propagation environments, an urban and a sub-urban one, against simulated values based on typical theoretical assumptions. We conclude by explaining how these assumptions should be carefully taken into account and how they can affect simulation results and the performance of applications.**

I. Introduction

In a typical radio propagation application, a large-scale path loss model is used to predict the distance based losses the radio signal suffers from, as it traverses through the environment. The local propagation environment induces further variability beyond what is captured by the distance dependent model, usually called *shadow fading* or simply *shadowing*. Understanding the properties of shadowing is key to accurate radio propagation estimates, whether for performance analysis of wireless systems or for network planning, deployment and operation. The increased focus on accurate shadowing models is becoming important due to new schemes and work on spatially dense networks, such as femto-cellular deployments and network concepts based on relaying. In the literature shadow fading is almost universally modeled as a Gaussian random process that is *spatially correlated*, i.e., at nearby locations the propagation losses attributed to shadow fading tend to be similar. Further, this process is almost always assumed to have same structure (namely same mean, standard deviation, and spatial correlation structure) over the entire study region, that is, the underlying process is assumed to be *stationary* [1]–[3].

In this paper we study through extensive propagation measurements the validity of these assumptions. We have conducted two measurement campaigns, one in suburban and another in urban environment. These measurements cover together nearly 2000 individual measurement locations, which enables us to make a detailed study of the spatial structure of shadow fading. Based on these measurements, we study whether shadow fading can indeed be safely considered to be stationary in two different senses. First, we show that both the marginal distribution (defined by the mean and standard deviation) as well as the spatial correlation properties of shadow fading vary significantly within the measurement area. These results show that one should be very careful when using existing shadow fading models to represent realistic propagation environment.

We also complement this work by including theoretical simulations that are typically used in the literature when real measurements are not available, and contrast the results obtained from such simulations against our measurements. That would help on the direction of improving understanding differences between theoretical and real-case scenarios. We also show through examples how one should be careful when using simulations for theoretical work.

The rest of this paper is structured as follows. In Section II we provide an overview of the hardware configuration, measurement methodology applied and the analytical tools we used to produce the results. In Section III we look on the hypothesis of homogeneity of the shadowing field by looking on results of the measurement set. In Section IV we present briefly how theoretical approaches can be different from real propagation conditions, before concluding the paper in Section V.

II. Hardware, Configuration and Processing of the Measurements

In order to measure the shadow fading values at 2.6 GHz, we have measured the received power of a signal in known locations around a transmitter. We transmitted a known signal with a stable power and frequency, and the fast fading was properly averaged out as explained bellow, while conducting the measurements. Then, by fitting the path loss model to the acquired data, we extracted accurately the shadowing field. Our high spatially conducted measurements allow the analysis of the spatial correlations of the shadowing field. It was very important to make sure that the transmitted power was stable during all the measurements, in order to ensure that the recorded received power was only describing the channel

978-1-4799-4912-0/14/$31.00 ©2014 IEEE

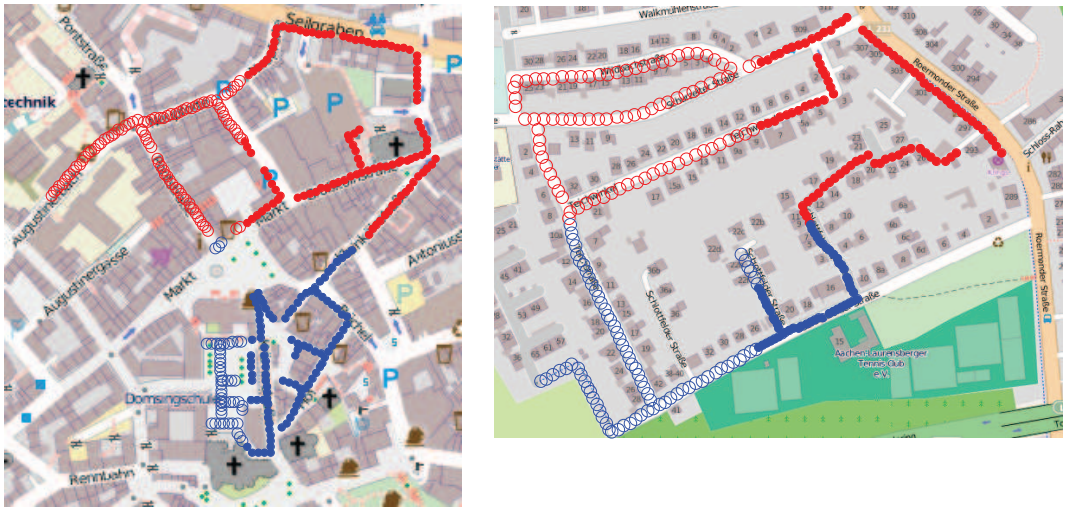

Fig. 1. Measurement points in urban and suburban environment. The colours differentiate between the upper (red) and lower (blue) regions. The symbols differentiate between left (circles) and right (dots) regions.

TABLE I
MEASUREMENT POINTS

Area	Total measurement points	Upper Part	Lower Part	Left Part	Right Part
Urban	923	512	411	504	419
Suburban	954	568	386	495	459

response. Moreover, for such a measurement campaign, the density of the measurement points and localization accuracy need to be high enough to resolve the underlying spatial characteristics of the field. The localization accuracy should be less than two meters, so as our measurement density to be much lower than the expected decorrelation distance [4]. GPS localization does not provide constantly sufficient accuracy and thus a high resolution map-based approach was used. The maps used, acquired by the Geographical reference data of the Municipalities and Federal State of North-Rhine Westphalia, provide a $20\,\mathrm{cm}$ position accuracy.

The transmitter consists of a signal generator that produces a continuous wave. The signal is amplified, with a class A amplifier and transmitted through an omnidirectional biconical antenna. We took special care for the antenna selection and we have chosen two highly omnidirectional antennas (Schwarzbeck SBA 9113) same for the transmitter and the receiver.

The receiver is composed of a spectrum analyzer, configured to capture precisely the transmitted signal, connected to a laptop that controls, timestamps and save the measurements. The hardware setup, the components comprising the transmitter and receiver used for these measurements as well as the extensive calibration tests and in-situ measurements done to ensure unbiased measurement collection and the stability of the transmitted power, are described extensively in [5].

Two different measurement campaigns took place in two different environments, a suburban and an urban one under non-line-of-sight (NLOS) conditions. As suburban environment was considered a suburb of Aachen, where family houses with one to three floors are the dominant type of buildings. The urban environment measurements, took place at the city-centre of Aachen, where high buildings are the dominant type of structures. For the suburban environment the transmitter was deployed on the rooftop of the premises of Institute for Networked Systems in Aachen, Germany. This is a five-storey office building that is also used by cellular providers as a base station site, whereas the transmitter in the urban case was deployed next to one of the main premisses of RWTH Aachen University, in a seven-store building also used by cellular system providers as base station site. The measurement locations were in the range of 150-$700\,\mathrm{m}$ away from the transmitter. In both measurement campaigns, we followed the same measurement procedure and we also kept logbooks to track the overall progress. The measurement points had an inter-distance of $2\,\mathrm{m}$. In order to extract the shadowing field from the received power, we had first to average out the effect of multipath and small scale fading. Based on the methodology described in [6], the local average power of a signal in a certain point can be measured by averaging 36 i.i.d. measurements taken along a distance of 40λ, that is equal to $4.6\,\mathrm{m}$ for the frequency of $2600\,\mathrm{MHz}$ used in the measurement. Similar techniques are also reported in the literature [7], [8] even though this is not always precisely described.

Measuring 36 positions in a distance of $4.6\,\mathrm{m}$ for every measurement point and having measurement points separated

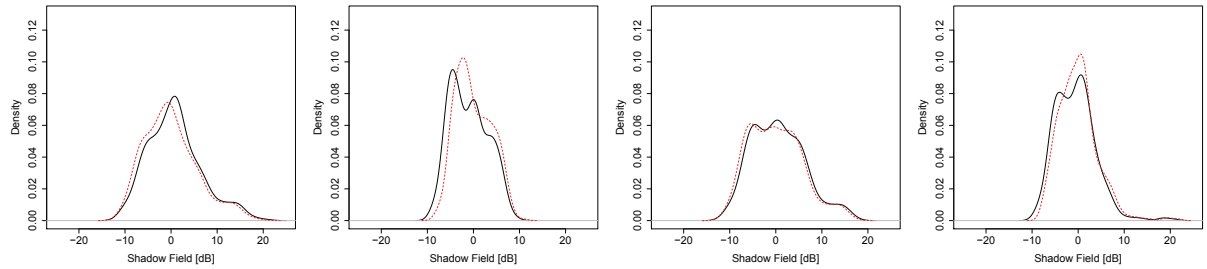

(a) Upper part, Urban (b) Lower part, Urban (c) Left part, Urban (d) Right part, Urban

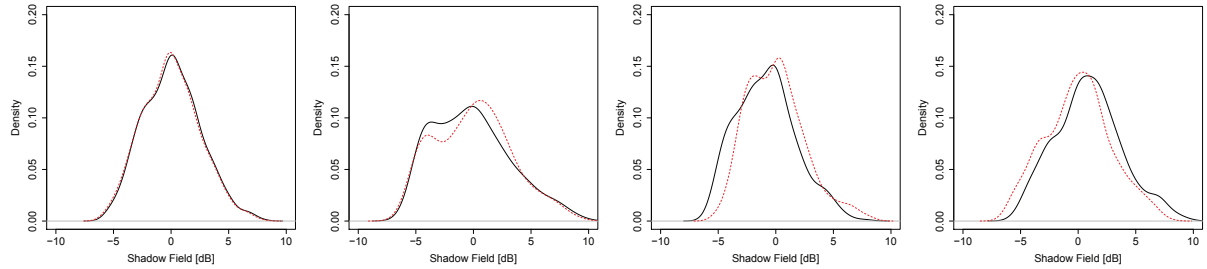

(e) Upper part, Suburban (f) Lower part, Suburban (g) Left part, Suburban (h) Right part, Suburban

Fig. 3. Partial marginal distributions for both global (black full line) and local (red dashed line) fit cases, for the urban and suburban environments.

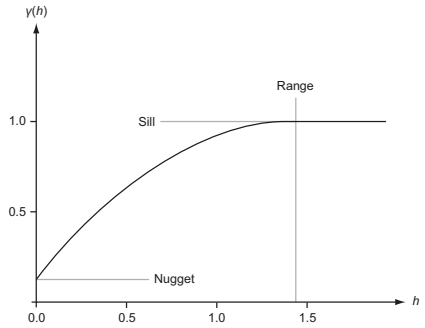

Fig. 2. Key features of a semivariogram (adapted from [9]).

by $2\,\mathrm{m}$ would lead to some positions that would be coinciding for two different measurement points. This would increase the correlation between the adjacent measurement points and would bias our analysis. In order to avoid an artificially higher correlation due to the above mentioned way of measuring, we took 200 measurements while moving in the range of $4.6\,\mathrm{m}$, for every measurement point. In that case the measurements start randomly in different positions while walking and the probability of two coinciding measurements in the same position for different measurement points is low. As we want to measure the local average power, we employ RMS energy detection as our main acquisition method. More about our acquisition method can be found in [5].

The analysis of the collected data starts with the extraction of the shadow field. The log-distance path loss model is fitted to the measured received power. The mathematical description of the log-distance path loss model is described as

$$P_r\,(\mathrm{dBm}) = c\,(\mathrm{dBm}) + 10\gamma \log_{10}(d_i) + Shadowing\,(\mathrm{dB}), \tag{1}$$

where $P_r\,(\mathrm{dBm})$ is the measured received power, d_i is the distance between transmitter and receiver and $c\,(\mathrm{dBm})$ denotes the transmitted power in addition to the gains for the antennae and any losses due to the transmitter and receiver systems. Finally around the median value there is an uncertainty modeled as normal distributed random variable, in the logarithmic scale, depicted here as $Shadowing\,(\mathrm{dB})$. The fast fading components is already removed with the measurement methodology already described. The path loss exponent, γ, and the constant c are evaluated through linear fitting and the shadowing is then extracted as the residuals of the fit, that is:

$$Shadowing\,(\mathrm{dB}) = P_r\,(\mathrm{dBm}) - (c + 10\gamma \log_{10}(d_i)) \tag{2}$$

Next step to the extraction of the shadow field, is the geostatistical analysis of it. There are various tools used for the spatial analysis of a random field. In this work we use the semivariogram or variogram due to its useful statistical properties [10]. The semivariogram shown in Fig. 2 is describing the spatial correlations of a spatial random field and it is equal to

$$\gamma(x_i, x_j) = \frac{1}{2}\,\mathrm{Var}(Z(x_i) - Z(x_j)), \tag{3}$$

where Var is the variance, $Z(*)$ is the random field, which for our case is the spatially correlated shadow fading and x_i, x_j are two measurement locations. When the distance between two measurement locations converges to zero (i.e. in Fig. 2, $h = 0$) then the variance also converges to zero, as the

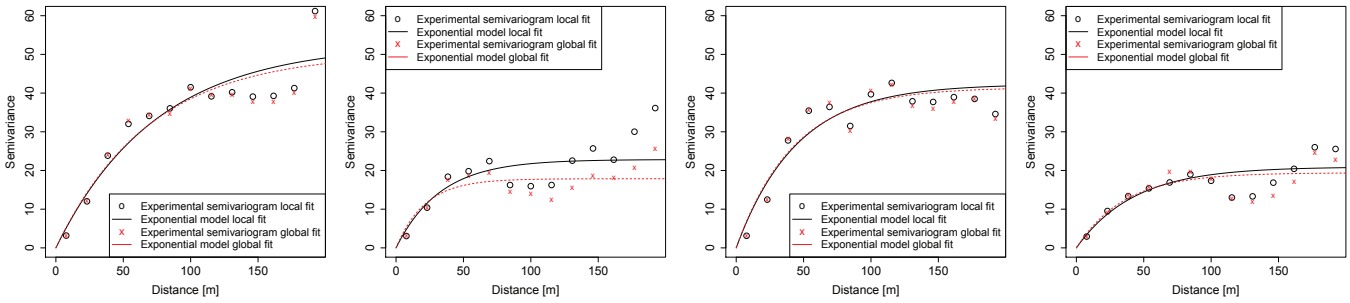

(a) Upper part, Urban (b) Lower part, Urban (c) Left part, Urban (d) Right part, Urban

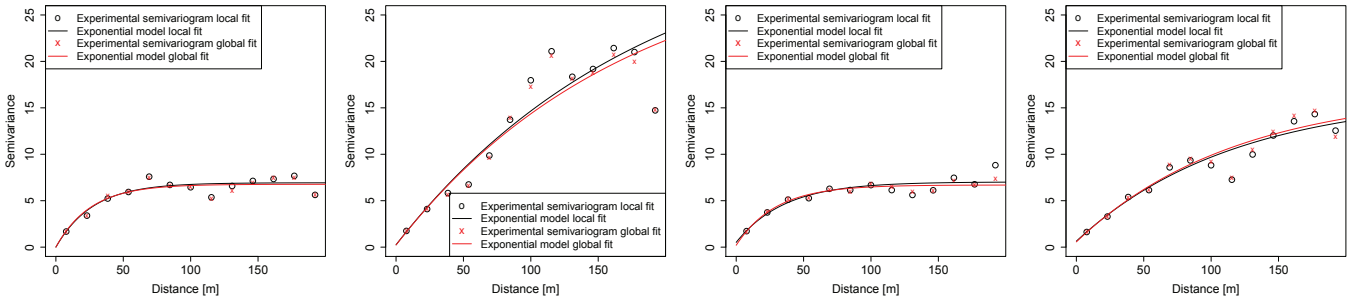

(e) Upper part, Suburban (f) Lower part, Suburban (g) Left part, Suburban (h) Right part, Suburban

Fig. 4. Partial experimental variograms and their respective exponential fits for the urban and suburban environment.

semivariogram describes the variance of the same realization. If there is a discontinuity in the origin of the semivariogram then it is called *nugget* and depicts noise in the measurements. On the other hand, as the distance between the points go to infinite, the semivariogram approaches the variance of the field and this is depicted as a plateau in the graph of a semivariogram, that is called *sill*. The distance in which the two realizations of the field are not correlated anymore is called *range*. In the case of asymptotic semivariograms equivalent of the range is the *practical range* that is the distance in which the correlation is equal to 0.05.

For the spatial analysis of a shadowing field we calculate the variance collecting all measurements where the pairs are at specified distances. This way the experimental semivariogram is created. The maximum distance of the semivariogram, i.e. the maximum distance between two measurement points that contribute to the semivariogram, is set to be equal to $250\,\mathrm{m}$, that is a distance that allows enough pairs to exist in every bin of the experimental semivariogram.

Towards the characterization of the spatial correlation of the shadowing field, semivariograms with theoretical correlation functions are fitted to the experimental semivariograms, so as to extract through regression the best estimated values for the above mentioned parameters. For the simulation and spatial analysis part of this paper, we used the *geoR* of R software [11], as it can model a Gaussian random field (a Gaussian random process assigned in certain locations in an area with an underlying spatial correlation) by using the autocorrelation functions and the semivariograms, so as to model the shadowing field.

III. Homogeneity of Shadow Fading

In this section we study the validity of homogeneity assumption, which is typically made for a shadowing field [12], [13]. We do that by splitting the measurement points into four sub-regions as is depicted in Fig. 1 for the two propagation environments. The split is done in respect to the center of the area that the measurements took place for every case. According to the homogeneity assumption, each sub-region should have the same shadowing distribution and correlation properties, or at least very similar, as always errors are introduced from the measurement procedure. Moreover, for reasons of completeness we have included two different approaches for the shadowing extraction and analysis. According to the first one we fitted the distance propagation loss model for all the measurement points and then we extracted the shadowing. For the second approach, we divided first the measurement points to four regions. Then each sub-region was separately fitted as an independent set of data to the path loss model and the shadowing field was extracted. The analysis of the first concept is always depicted in black continuous lines on all the graphs and from now on it will be called as *global fit*. The second technique used is depicted in red dashed lines on all the graphs and it will be called throughout this work as *local fit*.

The marginal distributions of the urban and suburban environments for the global and local fit for the four sub-regions are depicted in Fig. 3 show that the homogeneity assumption is not always justified, as the depicted graphs seem not to come from the same distribution, but exhibit high differences. More specifically, the urban marginal distributions in Fig. 3a, 3c, 3d show heavier tails than the normal distribution, that depicts a different variance and dispersion of the data. In all the cases of the urban environment, the local and the global average do not have a notable difference. On the other hand, for the suburban region the figures depict a more similar marginal distribution for the upper, left and right sub-regions (Fig. 3e, 3g, 3h), that can be explained by the fact that in such an environment the shadow field tends to have a more stable marginal distribution. In contrast to the urban case, the local and global fits in the suburban environment do not provide a different shape in the marginal distribution but slightly different dispersion of data and mean value (Fig. 3h).

Fig. 4 depicts the experimental semivariograms, along with the exponential fits of it, for all the sub-regions and for both environments. In the urban environment case, we see some similarity between the semivariograms for the upper and left sub-regions and the lower and right sub-regions. Despite those similarities, the sill and the practical ranges are not similar. For example the practical range for the upper sub-region is $207.39\,\mathrm{m}$ and $223.10\,\mathrm{m}$ for the local and the global fits respectively while the practical range for the left sub-region is estimated to be $127.34\,\mathrm{m}$ for the local fit and $134.29\,\mathrm{m}$ for the global fit. In the suburban environment, less fluctuations were found with Fig. 4e, 4g being very similar. The Fig. 4f, 4h also look to describe same type of structure but they still vary a lot in terms of correlation distance. Suburban environment seem to have less fluctuations in terms of propagation dynamics. However, we note that the theoretical models and simulations should take into account that even suburban environments have its own dynamics.

IV. Theoretical Work Limitations

Finally, we provide a brief, preliminary analysis on how some of the currently adopted simpler theoretical simulation tools may be suboptimal compared to the data driven models. Here we only discuss preliminary results and leave the extended work for the future. In order to study the situation, we generated 100 random field realizations with the same spatial sizes as our measurements, we generated 100 random field realizations with the same dimensions, of the urban area we measured, namely a $435 \times 388\,\mathrm{m}^2$ area and on the same locations as our measurements where done. Finally, we found the best matching simulated random field realization to our measurements. This is done so that we do not compare extreme cases from these two different sets, which would lead to many outliers and thus negatively biased comparison.

Comparing the results of Fig. 5 with the respective Fig. 3a, 3b, 3c and 3d, one notices that the marginal distribution per locality differs as expected. Theoretical models can not, of course, capture precise real site dynamics. However, the calculated marginal distributions for the simulated maps (Fig. 5) show clearly that when we split the analysis on the four sub-regions, the Gaussian characteristics of the shadowing field are much more retained. Thus there are also larger scale differences due to anisotropy that should be modeled in the future simulation based work, as such anisotropies can have a significant effect when modelling high density or directive networks. Dispersion of values is the same for the four sub-regions and also the mean value has almost the same density for the four cases. As we already mentioned none of these two characteristics were found on the propagation measurements. Simulated maps seem to lack the ability to describe precisely site specific content that is useful though for real deployments. Moreover the local fits in Fig. 5 provide even better Gaussian characteristics. We conclude this section by presenting, in Fig. 6, the variograms of the simulated data, for the four sub-regions for the local and global fit cases. All four regions show more similar covariance structure than the real data analysis shows. Finally, it seems that that the simulation outcomes are not consistent and do not always agree with the reality. Overall these examples show that the site specific dynamics can have a significant enough impact so that in the future work based on simulations should rely on more sophisticated variance structures and models so that Monte Carlo ensembles would become more realistic. This is especially important as taking into account shadowing correlations in the context of the next generation networks, cognitive radios, and shared spectrum access is becoming more important.

V. Conclusions

We have shown that some of the common assumptions of the shadowing fields should be used very carefully. The assumption that the shadowing fields are homogeneous do not seem to hold universally. Especially in urban cases, where the radio propagation can vary vastly between different regions, this assumption may not hold and should be taken into account when conducting Monte Carlo simulations or theoretical studies. We have also shown that for a specific region slight changes in the coefficients of the distance based losses, do not alter significantly spatial statistics thus reducing calculation overhead for REM and coverage database driven applications.

In real-world applications, the site specific dynamics can not be always available during modelling and design phase of a new system. This work has shown first that theoretical work should avoid over generalizations and one should allow some space for dynamics, uncertainty, and increased variance in parameters due to this. In our future work we plan to quantify this more closely, so that useful design rules could be provided to community for their modelling purposes.

The conducted measurement campaign also provides insights on the shadowing correlations at 2.6 GHz frequency, which is very close to ISM-and future LTE femtocell frequency bands. The results show that the shadowing correlation is quite strong and due to the high frequency one has assume also that non-isotropic correlation is often present at the level

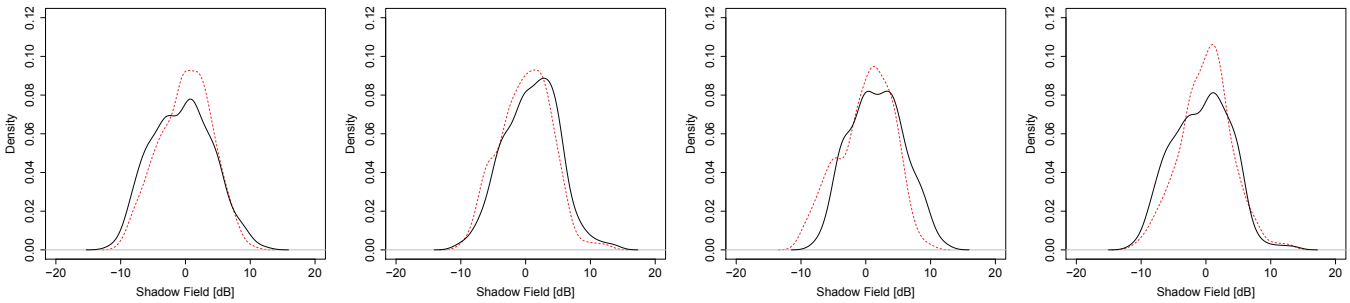

(a) Upper part, Simulated (b) Lower part, Simulated (c) Left part, Simulated (d) Right part, Simulated

Fig. 5. Marginal Distributions of the simulated random field, for local (red dashed line) and global (black full line) fit cases in urban environment.

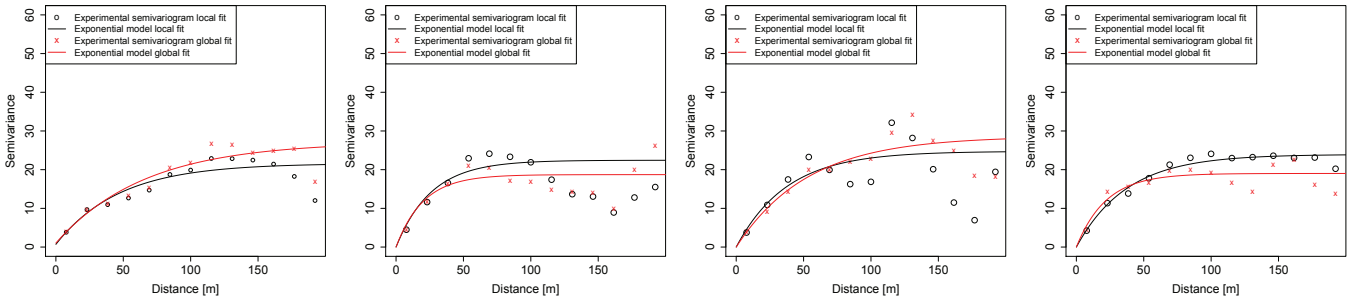

(a) Upper part, Simulated (b) Lower part, Simulated (c) Left part, Simulated (d) Right part, Simulated

Fig. 6. Experimental Variograms with their respective exponential fits, for local (red dashed line) and global (black full line) fit simulations in urban environment.

that has not been common in the case of earlier outdoor networks. The strong correlations, however, also provide opportunities that can be used to enhance efficiency through a clever radio resource management algorithms and spatial processing techniques. The paper shows that there is still a lot to do on understanding better the shadowing correlation statistics both theoretically and experimentally. We believe that this results necessitate a further research both in theoretical and practical domain.

Acknowledgement

The authors would like to thank RWTH Aachen University and the German Research Foundation (Deutsche Forschungsgemeinschaft, DFG) for providing financial support through the UMIC research centre. One of us (PM) has also benefited from RWTH Research Fellowship funded through excellence initiative of German Federal and State Governments

References

[1] V. Graziano, "Propagation correlations at 900 MHz," *Vehicular Technology, IEEE Transactions on*, vol. 27, no. 4, pp. 182–189, 1978.

[2] Y. Zhang, J. Zhang, D. Dong, X. Nie, G. Liu, and P. Zhang, "A Novel Spatial Autocorrelation Model of Shadow Fading in Urban Macro Environments," in *Global Telecommunications Conference, 2008. IEEE GLOBECOM 2008. IEEE*, 2008, pp. 1–5.

[3] K. Butterworth, K. Sowerby, and A. Williamson, "Correlated shadowing in an in-building propagation environment," *Electronics Letters*, vol. 33, no. 5, pp. 420–422, 1997.

[4] M. Gudmundson, "Correlation model for shadow fading in mobile radio systems," *Electronics letters*, vol. 27, no. 23, pp. 2145–2146, 1991.

[5] N. Perpinias *et al.*, "Measurements of Shadow Correlations in a Suburban Environment on the 485 MHz Band," in *VTC Fall 2013 in Las Vegas*, 2013.

[6] W. C. Y. Lee, "Estimate of local average power of a mobile signal." *IEEE Trans. on Vehicular Technology*, vol. 34, no. 1, pp. 22–27, 1985.

[7] H. Arnold, D. Cox, and R. Murray, "Macroscopic diversity performance measured in the 800 MHz portable radio communications environment," *IEEE Transactions on Antennas and Propagation*, vol. 36, no. 2, pp. 277–281, 1988.

[8] E. Perahia, D. Cox, and S. Ho, "Shadow fading cross correlation between basestations," in *Vehicular Technology Conference, 2001. VTC 2001 Spring. IEEE VTS 53rd*, vol. 1, 2001, pp. 313–317 vol.1.

[9] A. Palaios, J. Riihijärvi, O. Holland, A. Achtzehn, and P. Mähönen, "Measurements of Spectrum Use in London: Exploratory Data Analysis and Study of Temporal, Spatial and Frequency-Domain Dynamics ," in *Proc. of IEEE DySPAN 2012*, October 2012.

[10] N. A. Cressie, *Statistics for Spatial Data.* John Wiley and Sons., 1993. Revised Edition.

[11] P. Ribeiro Jr. and P. J. Diggle, "geoR: A package for geostatistical analysis," *R-NEWS*, vol. 1, 2001.

[12] S. Szyszkowicz, H. Yanikomeroglu, and J. Thompson, "On the Feasibility of Wireless Shadowing Correlation Models," *Vehicular Technology, IEEE Transactions on*, vol. 59, no. 9, pp. 4222–4236, 2010.

[13] J. Zhang and V. Aalo, "Effect of macrodiversity on average-error probabilities in a Rician fading channel with correlated lognormal shadowing," *Communications, IEEE Transactions on*, vol. 49, no. 1, pp. 14–18, 2001.